Deformation effects in ^{56}Ni nuclei produced in ^{28}Si+^{28}Si at 112 MeV

C. Bhattacharya,* M. Rousseau, C. Beck,† V. Rauch, R. M. Freeman, D. Mahboub,‡ R. Nouicer,§ P. Papka, and O. Stezowski‖
Institut de Recherches Subatomiques, UMR7500, Institut National de Physique Nucléaire et de Physique des Particules - Centre National de la Recherche Scientifique/Université Louis Pasteur, 23 rue du Loess, B.P. 28, F-67037 Strasbourg Cedex 2, France

A. Hachem and E. Martin
Université de Nice-Sophia Antipolis, F-06108 Nice, France

A. K. Dummer¶ and S. J. Sanders
Department of Physics and Astronomy, University of Kansas, Lawrence, Kansas 66045

A. Szanto De Toledo
Departamento de Física Nuclear, Instituto de Física da Universidade de São Paulo, C.P. 66318-05315-970 - São Paulo, Brazil
(Received 21 May 2001; published 20 December 2001)

Velocity and energy spectra of the light charged particles emitted in the ^{28}Si(E_{lab}=112 MeV)+^{28}Si reaction have been measured at the Strasbourg VIVITRON Tandem facility. The ICARE charged particle multidetector array was used to obtain exclusive spectra of the protons and α particles in the angular range 15°–150° and to determine the angular correlations of these particles with respect to the emission angles of the evaporation residues. The experimental data are analyzed in the framework of the statistical model. The exclusive energy spectra of α particles emitted from the ^{28}Si+^{28}Si compound system are generally well reproduced by Monte Carlo calculations using spin-dependent level densities. This spin dependence approach suggests the onset of large nuclear deformation at high spin. A reanalysis of previous α-particle data from the ^{30}Si+^{30}Si compound system, using the same spin-dependent parametrization, is also presented in the framework of a general discussion of deformation effects in the $A_{CN}\approx 60$ mass region.

DOI: 10.1103/PhysRevC.65.014611 PACS number(s): 25.70.Gh, 25.70.Jj, 24.60.Dr

I. INTRODUCTION

In recent years, there have been a number of experimental and theoretical studies [1] aimed at understanding the decay of light compound nuclei (CN) and dinuclear systems ($A_{CN} \leqslant 60$) formed through low energy heavy-ion reactions ($E_{lab} \leqslant 10$ MeV/nucleon). In most of the reactions studied, the properties of the observed, fully energy damped yields have been successfully explained in terms of either a fusion-fission (FF) mechanism or a heavy-ion resonance behavior [1–3]. The strong resonancelike structures observed in elastic and inelastic excitation functions of ^{24}Mg+^{24}Mg [2] and ^{28}Si+^{28}Si scatterings [3] have been suggestive of the presence of shell stabilized, highly deformed configurations in the ^{48}Cr and ^{56}Ni $N=Z$ dinuclear systems, respectively [1]. The investigation of the structure of the doubly magic ^{56}Ni nucleus is particularly interesting, with the recent observation [4] in this system of deformed bands that may be the precursors of large deformation or superdeformation behavior in the $A_{CN}\approx 60$ mass region [5,6].

In a recent experiment using the EUROGAM phase II γ-ray spectrometer, we have investigated [7,8] the possibility of preferential population of highly deformed bands in the symmetric fission channel of the ^{56}Ni* CN, produced through the ^{28}Si+^{28}Si reaction at $E_{lab}=112$ MeV, which corresponds to the energy of the conjectured $J^{\pi}=38^{+}$ quasimolecular resonance [3]. Some evidence for this behavior was observed [7,8], but should be confirmed to be more conclusive.

The present work involves the search for the possible occurrence of highly deformed configurations of the ^{56}Ni* CN produced in the ^{28}Si+^{28}Si reaction. Light charged particles (LCP) emitted at the resonance energy [7,8] of $E_{lab}=112$ MeV, and in-plane coincidences of the LCP's with both evaporation residues (ER) and FF fragments have been measured. The LCP's emitted during the CN decay processes carry information on the underlying nuclear shapes and level densities. In particular, new information on nuclear structure far above the yrast line can be obtained from their study by a comparison with statistical model calculations [9]. The LCP's emitted from FF fragments may provide the deformation properties of these fragments. Studies of nuclear shapes based on evaporated LCP spectra have evoked considerable interest and controversy [9–18]. For example, an extremely large nuclear deformation suggested in the decay of the ^{60}Ni* CN [11], formed in the reaction ^{30}Si+^{30}Si at E_{lab}

*Permanent address: VECC, 1/AF Bidhan Nagar, Kolkata 64, India.
†Corresponding author. Email address: christian.beck@ires.in2p3.fr
‡Present address: University of Surrey, Guildford GU2 7XH, U.K.
§Present address: Department of Physics, University of Illinois at Chicago, Chicago, IL 60607-7059.
‖Permanent address: IPN Lyon, F-69622 Villeurbanne, France.
¶Present address: Triangle Universities Nuclear Laboratory, University of North Carolina, Durham, NC 27708-0308.

$=120$ MeV, was not supported by the statistical model analysis of Nicolis and Sarantites [19].

In this paper we will focus on the LCP's found in coincidence with ER's. These data will be analyzed with the CACARIZO statistical model code [9]. Section II describes the experimental procedures. In Sec. III we present the data analysis of the exclusive ^{28}Si+ ^{28}Si data (part of the experimental results presented here in detail have already been briefly reported elsewhere [20–24]). The statistical model calculations are compared to the experimental data in Sec. IV in the framework of a general discussion of deformation effects in the $A_{CN}\approx 60$ mass region. This section includes a reanalysis of existing α-particle data from the ^{30}Si+ ^{30}Si reaction previously measured by La Rana *et al.* [11] using a consistent set of input parameters fitting both ^{28}Si+ ^{28}Si and ^{30}Si+ ^{30}Si α-particle spectra. We end with a summary of our results in Sec. V.

II. EXPERIMENTAL PROCEDURES

The experiment was performed at the IReS Strasbourg VIVITRON Tandem facility, using a 112 MeV ^{28}Si beam incident on a self-supported 180 μg/cm^2 thick ^{28}Si target prepared at IReS. Additional targets of natural ^{12}C, gold, and Formvar were irradiated for calibration, background determination, and normalization purposes. The elemental compositions of the ^{28}Si target was accurately determined at IReS using Rutherford backscattering (RBS) techniques with ^{1}H and ^{4}He beams provided by the 4 MV Van de Graaff accelerator [22]. The main target contaminants were C and O, each contributing less than 2% to the total number of atoms in the target, and Cu. Because of the relatively low beam energy with respect to the barrier energy for Cu, this contaminant is not expected to affect our results. The natural C target was used to obtain the background correction for this element. These corrections were found to be relatively small.

Both the heavy ions and their associated LCP's were detected using the ICARE charged particle multidetector array [25]. The heavy fragments (ER, quasielastic, deep-inelastic, and FF fragments) have been detected in eight gas-silicon hybrid telescopes (IC), each consisting of an ionization chamber, with a thin Mylar entrance window, followed by a 500 μm thick Si(SB) detector. The IC's were located at $\Theta_{lab}=\pm 15°$, $-20°$, $\pm 25°$, $-30°$, $-35°$, and $-40°$ in two distinct reaction planes (for each plane, the positive and negative angles refer to the opposite and same side of the beam as the heavy-ion IC detector, respectively). The in-plane detection of coincident LCP's was done using four triple telescopes [40 μm Si, 300 μm Si, and 2 cm CsI(Tl)] placed at forward angles ($\Theta_{lab}=+15°$, $+25°$, $+35°$, and $+45°$), 16 two elemental telescopes [40 μm Si, 2 cm CsI(Tl)] placed at forward and backward angles ($+40° \leqslant \Theta_{lab} \leqslant +115°$), and finally two other IC's telescopes placed at the most backward angles $\Theta_{lab}=+130°$ and $+150°$. The IC's were filled with isobutane and their pressures were kept at 30 Torr at backward angles and 60 Torr at forward angles, respectively, for detecting light fragments and heavy fragments. The acceptance of each telescope was defined by thick aluminum collimators.

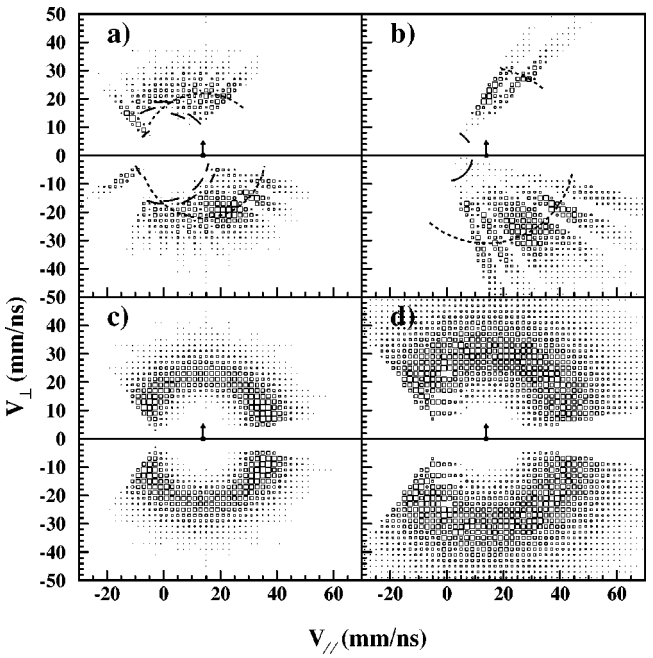

FIG. 1. Two-dimensional scatter plots of Galilean invariant cross sections $(d^2\sigma/d\Omega dE)p^{-1}c^{-1}$ of α particles (a) and protons (b), respectively, in the $(V_{\parallel},V_{\perp})$ plane for the ^{28}Si(112 MeV) + ^{28}Si reaction. The experimental detector thresholds are drawn along the laboratory angles of each telescope. (c) and (d) are the corresponding statistical model calculations discussed in the text. The dashed circular arcs are centered on the velocity of the center of mass indicated by the arrows.

The calibration of the ICARE multidetector array was done using radioactive ^{228}Th and ^{241}Am α sources, a precision pulser, and elastic scattering of 112 MeV ^{28}Si from ^{197}Au, ^{28}Si, and ^{12}C targets in a standard manner. In addition, α particles emitted in the ^{12}C(^{16}O, ^{4}He)^{24}Mg* reaction at $E_{lab}(^{16}O)=53$ MeV provide known α particle energies from the decay of ^{24}Mg excited states thus allowing for the calibration of the backward angles detectors [22,25]. The proton calibration was done using scattered protons from Formvar targets using both the ^{28}Si and ^{16}O beams. More details on the experimental setup of ICARE and on the analysis procedures can be found in Refs. [22,24,25], and references therein.

III. DATA ANALYSIS AND EXPERIMENTAL RESULTS

The velocity contour maps of the LCP Galilean invariant differential cross sections $(d^2\sigma/d\Omega dE)p^{-1}c^{-1}$ as a function of the LCP velocity provides an overall picture of the reaction pattern. Figures 1(a) and 1(b) show such two-dimensional scatter plots for inclusive α particles and protons, respectively. For a sake of clarity the velocity cut offs arising from the detector low-energy thresholds are indicated for each telescope. $V_{\parallel}$ and $V_{\perp}$ denote laboratory velocity components parallel and perpendicular to the beam, respectively. Figures 1(c) and 1(d) are the corresponding plots as calculated by the statistical model discussed in the following section. The dashed circular arcs, centered on the center of

mass $V_{\text{c.m.}}$ and defined to visualize the maxima of particle velocity spectra, describe the bulk of data rather well as can be observed for instance for the proton velocity spectra. They have radii very close to the Coulomb velocities of α particles and protons in the decay of $^{56}\text{Ni}^* \rightarrow {}^{52}\text{Fe} + {}^{4}\text{He}$ and of $^{56}\text{Ni}^* \rightarrow {}^{55}\text{Co} + {}^{1}\text{H}$, respectively. The apparent worsening of the agreement between the experimental and calculated α-particle spectra results at larger angle by the relatively large low-energy thresholds of the most backward-angle telescopes. Despite these deviations, the spectra can be understood by assuming a sequential evaporative process and successive emission sources starting with the thermally equilibrated ^{56}Ni* CN until the final source characterized by a complete freeze-out of the residual nucleus. The invariant cross section contours fall around the dashed circular arcs centered at the CN recoil velocity $V_{\text{CN}} = V_{\text{c.m.}}$, and represent the isotropic emission patterns to be expected for a fusion-evaporation mechanism after full-momentum transfer and complete fusion (CF). LCP's emitted from direct reactions or from a prethermalization emission process would have manifested themselves as even stronger deviations from the dashed circular arcs, as shown at much higher bombarding energies $E(^{28}\text{Si}) = 12.4$, 19.7, and 30 MeV/nucleon, for the $^{28}\text{Si} + {}^{28}\text{Si}$ reaction [26,27]. In these early works [26,27] only a few preequilibrium LCP's have been shown to be emitted prior to fusion at the lowest energy $E(^{28}\text{Si}) = 12.4$ MeV/nucleon [26,27], therefore the absence of a preequilibrium component at the present energy $E(^{28}\text{Si})$ of 4 MeV/nucleon is expected.

Figures 2(a) and 2(b) show the exclusive scatter plots of Galilean invariant differential cross sections in the $(V_{\parallel}, V_{\perp})$ plane, for α particles and protons measured in coincidence with all ER's ($20 \leqslant Z \leqslant 25$), identified in a IC detector located at $\Theta_{\text{lab}}^{\text{ER}} = -15°$. Figures 2(c) and 2(d) are statistical model predictions discussed in Sec. IV. As for the inclusive data, there is no bias due to direct or preequilibrium processes. Thus we are confident that essentially all the emitted particles are associated with a statistical de-excitation process arising from a thermalized source such as the ^{56}Ni CN. The energy spectra of these particles, presented next, are also strongly supportive of this conclusion.

Typical exclusive energy spectra of the corresponding α particles are shown in Fig. 3 at the indicated angles (from $\Theta_{\text{lab}}^{\text{LCP}} = +40°$ to $\Theta_{\text{lab}}^{\text{LCP}} = +65°$) for the $^{28}\text{Si} + {}^{28}\text{Si}$ reaction at $E_{\text{lab}}(^{28}\text{Si}) = 112$ MeV. The measured α particles are in coincidence with all ER's ($20 \leqslant Z \leqslant 25$) identified in the IC detector located at $\Theta_{\text{lab}}^{\text{ER}} = -15°$ (the IC's located at more backward angles have too low statistics for fusion-evaporation events to be used in the analysis). The spectral shapes of the coincident α particles are very similar to inclusive energy spectra but without low-energy, non-Maxwellian contributions, as shown in Fig. 6. All the spectra have Maxwellian shapes with an exponential fall-off at high energy which reflects a relatively low temperature ($T_{\text{slope}} \approx [8E_{\text{CN}}^*/A_{\text{CN}}]^{1/2} = 3.1$ MeV) of the decaying nucleus. The shape and high-energy slopes are also found to be essentially independent of angle in the c.m. system. These behaviors

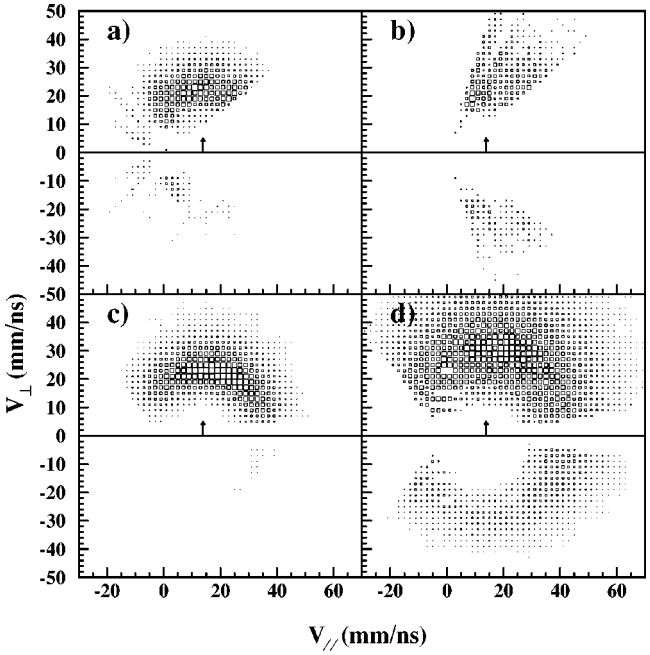

FIG. 2. Two-dimensional scatter plots of exclusive Galilean invariant cross sections $(d^2\sigma/d\Omega dE)p^{-1}c^{-1}$ of α particles (a) and protons (b), respectively, measured in coincidence with all ER's ($20 \leqslant Z \leqslant 25$) identified in a IC detector located at $\Theta_{\text{lab}}^{\text{ER}} = -15°$, as plotted in the $(V_{\parallel}, V_{\perp})$ plane for the $^{28}\text{Si}(112\ \text{MeV}) + {}^{28}\text{Si}$ reaction. (c) and (d) are the corresponding results of the statistical model calculations discussed in the text. The arrows indicate the center-of-mass velocity.

suggest, as for the velocity spectra, a statistical CN decay process.

The in-plane angular correlations of α particles and protons (measured in the $-115° \leqslant \Theta_{\text{lab}}^{\text{LCP}} \leqslant +115°$ angular range) in coincidence with all the ER's ($20 \leqslant Z \leqslant 25$), pro-

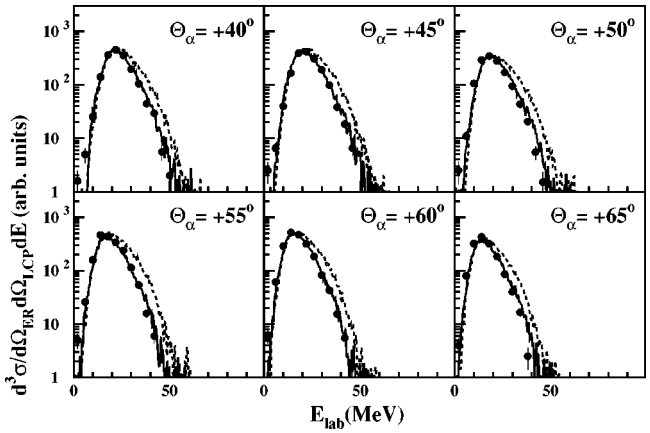

FIG. 3. Exclusive energy spectra of α particles in coincidence with all ER's ($20 \leqslant Z \leqslant 25$), identified in a IC detector located at $\Theta_{\text{lab}}^{\text{ER}} = -15°$, produced in the $^{28}\text{Si}(112\ \text{MeV}) + {}^{28}\text{Si}$ reaction. The experimental data are given in relative units by the solid points with error bars visible when greater than the size of the points. The dashed and solid lines are the results of statistical model calculations using parameter set A and set B, respectively, as discussed in the text.

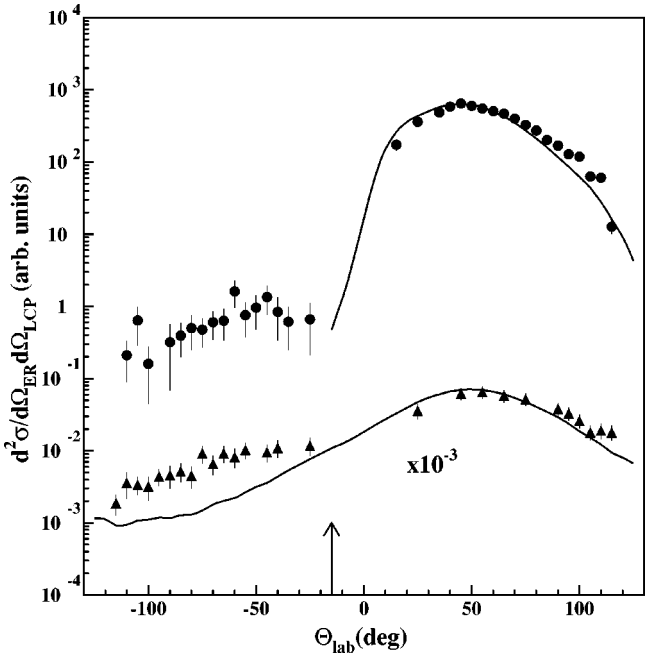

FIG. 4. In-plane angular correlation ($-115° \leqslant \Theta_{lab}^{LCP} \leqslant +115°$) of α particles (circles) and protons (triangles) in coincidence with all ER's ($20 \leqslant Z \leqslant 25$) produced in the ^{28}Si(112 MeV)+ ^{28}Si reaction and detected at $\Theta_{lab}^{ER} = -15°$ as shown by the arrow. The solid curves are the results of statistical model calculations using parameter set B as discussed in the text.

duced in the ^{28}Si(112 MeV)+ ^{28}Si reaction, are shown in Fig. 4. The angular correlations are peaked strongly on the opposite side of the ER detector located at $\Theta_{lab}^{ER} = -15°$ with respect to the beam. This peaking is the result of the momentum conservation. The solid lines shown in the figure are the results of statistical model predictions for CF and equilibrium decay using the code CACARIZO [9], as discussed in the next section.

IV. STATISTICAL MODEL CALCULATIONS AND DISCUSSION

The analysis of the data has been performed using CACARIZO [9], the Monte Carlo version of the statistical model code CASCADE [28]. The parameters needed for the statistical description, i.e., the nuclear level densities and the barrier transmission probabilities, are usually obtained from the study of light particle evaporation spectra. In recent years, it has been observed that statistical model calculations, using standard parameters, are unable to predict satisfactorily the shape of the α-particle energy spectra [9–18] with the measured average energies of the α particles found to be much lower than the corresponding theoretical predictions. In the present calculations as well as in previous studies [9,10,12–18], the transmission coefficients of all competing evaporation channels, including *n*, *p*, and α-particle emission, are generated from published optical model parameters for spherical nuclei. Several attempts have been made in the past few years to explain LCP energy anomaly either by changing the emission barrier or by using a spin-dependent level density. The change in the emission barriers and, correspondingly, the transmission probabilities affects the lower energy part of the calculated evaporation spectra. On the other hand, the high-energy part of the spectra depends critically on the available phase space obtained from the level densities at high spin. In hot rotating nuclei formed in heavy-ion reactions, the level density at higher angular momentum is spin dependent. The level density, $\rho(E,J)$, for a given angular momentum J and energy E is given by the well known Fermi gas expression

$$\rho(E,J) = \frac{(2J+1)}{12} a^{1/2} \left(\frac{\hbar^2}{2\mathcal{J}_{\rm eff}} \right)^{3/2} \frac{1}{(E-\Delta-T-E_J)^2} \times \exp\{2[a(E-\Delta-T-E_J)]^{1/2}\}, \quad (1)$$

where a the level density parameter is constant and set equal to $a = A/8$ MeV^{-1} (A is the mass number), T is the "nuclear" temperature, and Δ is the pairing correction, $E_J = (\hbar^2/2\mathcal{J}_{\rm eff})J(J+1)$ is the rotational energy, $\mathcal{J}_{\rm eff} = \mathcal{J}_0 \times (1 + \delta_1 J^2 + \delta_2 J^4)$ is the effective moment of inertia, $\mathcal{J}_0 = \frac{2}{5} AR^2 = \frac{2}{5} A^{5/3} r_0^2$ is the rigid body moment of inertia (r_0 is the radius parameter), and δ_1 and δ_2 are the deformability parameters defined in Refs. [9,10,12].

The angular momentum distribution used in the statistical model calculations depends on the diffusivity parameter ΔL and the critical angular momentum for fusion $L_{\rm cr}$. A fixed value of $\Delta L = 1\hbar$ is assumed for the calculations. The $L_{\rm cr}$ values were deduced based on observed complete fusion cross section. These values are shown in Table I for a number of systems with $46 \leqslant A_{\rm CN} \leqslant 60$. The same angular momenta value of $L_{\rm cr} = 34\hbar$ is found for both the ^{28}Si+ ^{28}Si [29–31] and ^{30}Si+ ^{30}Si [32,33] fusion reactions. Otherwise we have used the CASCADE parameters for the nickel isotopes (see Table 8 of Ref. [33]). The only parameters adjusted in the calculations were those directly associated with the system deformation, δ_1 and δ_2, the so-called deformability parameters.

In the present analysis we have chosen to follow the procedure proposed by Huizenga and collaborators [12]. No attempt was made to modify the transmission coefficients since it has been shown that the effective barrier heights are fairly insensitive to the nuclear deformation [12]. On the other hand, by changing the deformability parameters δ_1 and δ_2 one can simulate the spin-dependent level density [9,10,12] associated to a larger nuclear deformation. We understand that the deformation should be attenuated with the subsequent emissions, i.e., there is a readjustment of shape of the nascent final nucleus and a change of collective to intrinsic excitation during the particle evaporation process. In CACARIZO the nuclear deformation is not allowed to be maintained equal to that in the first step during the entire compound nucleus decay chain because the memory is lost after each single decay step. The CACARIZO calculations have been performed using two sets of input parameters: one with a standard set of the rotating liquid drop model [28] (RLDM) (parameter set A), consistent with the deformation of the finite-range rotating liquid drop model [34] (FRLDM), and another with a spin-dependent moment of inertia and larger

TABLE I. Typical quantities of the evaporation calculations performed using the statistical model code CACARIZO. The deformability parameters are taken either from the parameter set B for the systems studied in the present work or from similar fitting procedures for the other systems studied in the literature. The minor to major axis ratios b/a and the quadrupole deformation β values (for a symmetric oblate shape and a symmetric prolate shape, respectively) have been deduced from equations discussed in the text. Note that the β values given for ^{32}S+ ^{27}Al have been extracted assuming the L_{cr} as extracted at the highest bombarding energy.

Reaction	CN	Energy (MeV)	L_{cr} ($\hbar$)	δ_1	δ_2	b/a	β	References
^{28}Si+ ^{27}Al	^{55}Co	150	42	1.8×10^{-4}	1.8×10^{-7}	1.2/1.3	−0.44/0.46	[13]
^{28}Si+ ^{28}Si	^{56}Ni	112	34	1.2×10^{-4}	1.1×10^{-7}	1.5/1.6	−0.48/0.49	This work
^{35}Cl+ ^{24}Mg	^{59}Cu	260	37	1.1×10^{-4}	1.3×10^{-7}	1.6/1.7	−0.50/0.51	[18]
^{32}S+ ^{27}Al	^{59}Cu	100–150	27–39	2.3×10^{-4}	1.6×10^{-7}	1.4–2.0	−0.46/0.53	[9]
^{32}S+ ^{27}Al	^{59}Cu	100–150	27–42	1.3×10^{-4}	1.2×10^{-7}	1.5–2.2	−0.48/0.54	[19]
^{30}Si+ ^{30}Si	^{60}Ni	120	34	1.2×10^{-4}	1.1×10^{-7}	1.6/1.7	−0.49/0.50	This work

values for the deformability parameters (parameter set B). The RLDM parameter set A with small values given to deformability parameters ($\delta_1=7.6\times10^{-6}$ and $\delta_2=6.7\times10^{-8}$) produces a yrast line very close to the FRLDM predictions, as shown, for example, for the neighboring ^{59}Cu nucleus in Ref. [9] (see Fig. 1 of Ref. [9]). The final values of the deformability parameters, $\delta_1=1.2\times10^{-4}$ and $\delta_2=1.1\times10^{-7}$ given in Table I for the parameter set B, are rather large and yield a significant lowering of the corresponding FRLDM yrast line. They have been chosen in order to reproduce the exclusive data rather than the inclusive data (although they have almost identical spectral shapes especially in the high-energy region), the latter being possibly influenced for low-energy LCP's by small nonstatistical components resulting from inelastic collisions or breakup processes that are not accounted for in the statistical model calculations.

The dashed lines in Fig. 3 show the predictions of CACARIZO for ^{28}Si+ ^{28}Si using the parameter set A consistent with FRLDM deformation [34]. It is clear that the average energies of the measured α-particle spectra are lower than those predicted by these statistical model calculations. The same observation can be made in Fig. 5 for the inclusive ^{30}Si+ ^{30}Si data [11] which have been analyzed with the same parameters as used for the ^{28}Si+ ^{28}Si reaction (the corresponding inclusive ^{28}Si+ ^{28}Si data are also displayed in Fig. 6 for the sake of comparison). The solid lines of Figs. 3, 5, and 6 show the predictions of CACARIZO using the increased values of the deformability parameters (see parameter set B given in Table I). The agreement is considerably improved. For instance in Fig. 3 the shapes of the exclusive α-particle energy spectra are very well reproduced for ^{28}Si + ^{28}Si with parameter set B (solid lines) including the deformation effects. Furthermore and despite the fact that, for the inclusive α-particle spectra of the ^{28}Si+ ^{28}Si reactions of Fig. 6, there appears to be an excess of yield in the subbarrier energy data, the chosen parametrization of the moment of inertia does also a fairly good job. It may be mentioned that in the case of protons, as they carry away less angular momentum than α particles, their calculated energy spectra do not shift as the spin-dependent parametrization of the moment of inertia is introduced. The statistical model results using the two parameter sets reproduce equally well the experimental velocity spectra and angular correlations. The statistical model calculations displayed for protons on Figs. 1, 2, and 4 have been performed with parameter set B (solid lines of Fig. 4) including the deformation effects (calculations with parameter set A are not displayed). The deformability parameters for the other systems, given in Table I, were extracted using the same approach of fitting procedures [9,13,18,19] that was employed in the present work for the

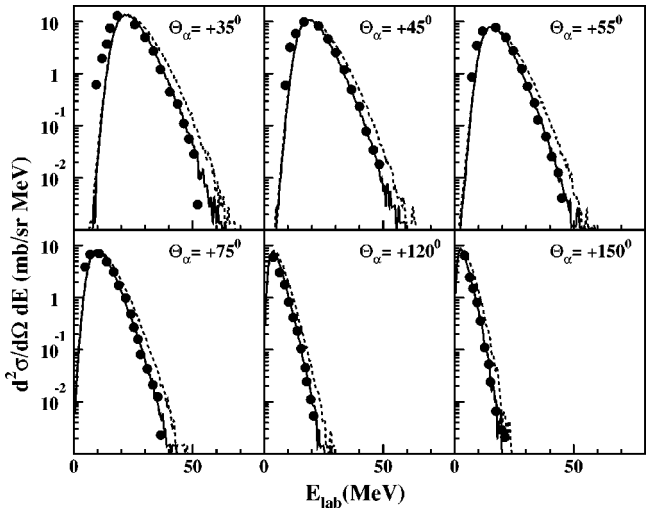

FIG. 5. Energy spectra of α particles produced in the ^{30}Si(120 MeV)+ ^{30}Si reaction. The data taken from Ref. [11] (solid points) are compared to the results of the statistical model calculations (the dashed and solid lines correspond to parameter set A and set B, respectively) discussed in the text.

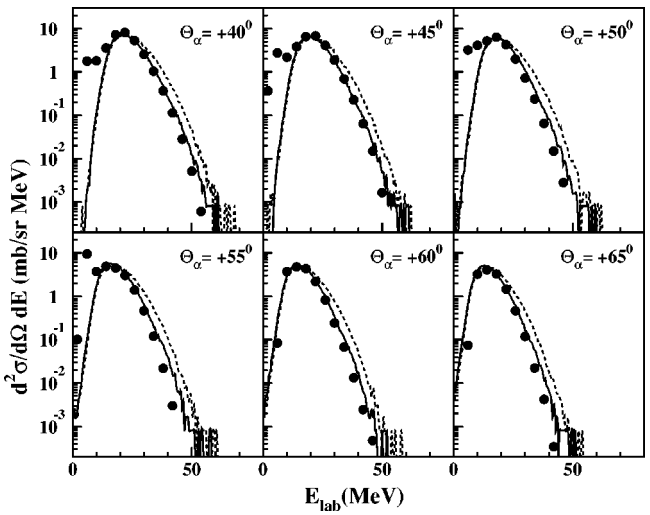

FIG. 6. Energy spectra of α particles produced in the ^{28}Si(112 MeV)+ ^{28}Si reaction. The inclusive cross sections are given as absolute values by the solid points with error bars visible when greater than the size of the points. The dashed and solid lines are the results of statistical model calculations using parameter set A and set B, respectively, as discussed in the text.

^{28}Si+ ^{28}Si and ^{30}Si+ ^{30}Si reactions.

The CACARIZO predictions shown in Figs. 1 and 2, also performed with the parameter set B given in Table I, reproduce the maxima of the inclusive and exclusive invariant cross sections quite well. This confirms that most of the yields have a statistical origin. This is consistent with the experimental alpha-to-proton ratio $R_{\alpha/p}^{\exp}=0.40\pm0.06$ which value is better predicted by calculations using parameter set B ($R_{\alpha/p}^{\mathrm{set}-B}=0.39$) than calculations using parameter set A ($R_{\alpha/p}^{\mathrm{set}-A}=0.48$). Parameter set A overestimate the alpha-to-proton ratio mainly because of first chance α particle. Parameter set B allows the emission of more nucleons in the cascade and the average emission step for α particles occurs later in the cascade. Thus the velocity plots, the spectral shapes, the angular correlations, and relative cross sections of α particle and proton emission are all reproduced correctly. On the other hand, the discrepancies observed at the most negative angles (between $\Theta_{\mathrm{lab}}^{\mathrm{LCP}}=-30°$ and $-110°$) of the in-plane angular correlations of Fig. 4, for protons and even more for α particles, are sometimes difficult to be understood as already stressed in Refs. [18,35]. The same disagreement is present with the calculations using parameter set A. However, it is seen that the shapes of the experimental angular correlations are well reproduced by the statistical theory for the positive angles, although a very small shift of $\Delta\Theta_{\mathrm{lab}}^{\mathrm{LCP}}=10$–$15°$ may improve the comparison.

In addition, it is interesting to note that for the ^{30}Si + ^{30}Si reaction the relative multiplicities of nucleons and α particles deduced from the experimental data [33] ($M_n^{\exp}=0.469\pm0.035$, $M_p^{\exp}=0.343\pm0.035$, and $M_\alpha^{\exp}=0.188\pm0.035$) are in better agreement with the calculations using the parameter set B ($M_n^{\mathrm{def}}=0.484$, $M_p^{\mathrm{def}}=0.312$, and $M_\alpha^{\mathrm{def}}=0.204$) than those using the parameter set A ($M_n^{\mathrm{LDM}}=0.459$, $M_p^{\mathrm{LDM}}=0.293$, and $M_\alpha^{\mathrm{LDM}}=0.248$).

As a whole, the present statistical model calculations describe rather well all the measured observables for both the ^{28}Si+ ^{28}Si and ^{30}Si+ ^{30}Si reactions, in contrast to other recent studies which have needed extra dynamical effects in the evaporative processes [16,17]. In order to better appreciate the magnitude of the possible deformation effects which are suggested by our chosen statistical model approach, one may express the effective moment of inertia as $\mathcal{J}_{\mathrm{eff}}=\frac{2}{5}MR^2=\frac{1}{5}M(b^2+a^2)$ with the volume conservation condition $V=\frac{4}{3}\pi abc$, where b and a are the major and minor axis, and c is the rotational axis of the compound nucleus. In the case of an oblate shape $a=b$ and $\mathcal{J}_{\mathrm{eff}}=\frac{2}{5}Ma^2$ and $V=\frac{4}{3}\pi a^2c$. The axis ratio is equal to $\delta=a/c=(1+\delta_1J^2+\delta_2J^4)^{3/2}$. In the case of a prolate shape $a=c$ and $\mathcal{J}_{\mathrm{eff}}=\frac{1}{5}M(b^2+a^2)$ and $V=\frac{4}{3}\pi a^2b$. We obtain the equation $1+(3-\gamma)x+3x^2+x^3=0$ with $x=(b/a)^2=\delta^2$ and $\gamma=8(1+\delta_1J^2+\delta_2J^4)^3$. The quadrupole deformation parameter β is equal to $\beta=1/\sqrt{5\pi}(\frac{4}{3}\delta+\frac{2}{3}\delta^2+\frac{2}{3}\delta^3+\frac{11}{18}\delta^4)$.

The minor to major axis ratios b/a and the values of the quadrupole deformation parameter β are shown for the systems tabulated in Table I. These quantities have been extracted from the fitted deformability parameters by assuming either a symmetric oblate shape or a symmetric prolate shape, respectively, with sharp surfaces [12]. All of the symmetric or near symmetric systems [13,18,19], for which the main parameters are listed in the table, appear to favor relatively large nuclear deformations. This can be contrasted with what is found for the asymmetric ^{12}C + ^{45}Sc reaction [17], where a standard statistical model calculation [17] is found to work well. The same conclusion was reached for the ^{28}Si+ ^{51}V reaction [14], another asymmetric system, and was confirmed for the very asymmetric system ^{16}O+ ^{54}Fe [16].

From this systematic analysis, it can be observed that the magnitude of the quadrupole deformation that can be deduced for both ^{28,30}Si+ ^{28,30}Si reactions is rather large: their parameter values are similar to the value obtained for the ^{32}S+ ^{27}Al reaction [9,19] but larger than the value corresponding to the ^{28}Si+ ^{27}Al reaction [13]. This leads to the striking conclusion that highly stretched configurations are required to account for the observed α-particle evaporation spectra. For ^{28}Si+ ^{28}Si the value of $\beta\approx0.5$ found for the quadrupole deformation parameter is consistent with the recent observation of very deformed bands in the doubly magic ^{56}Ni nucleus by standard γ-ray spectroscopy methods [4].

V. CONCLUSION

To summarize, the properties of the light charged particles emitted in the ^{28}Si+ ^{28}Si reaction at the bombarding energy $E_{\mathrm{lab}}(^{28}\mathrm{Si})=112$ MeV, which corresponds to the ^{56}Ni excitation energy of the conjectured $J^\pi=38^+$ quasimolecular resonance [7,8], have been investigated using the statistical model. The measured observables such as velocity distributions, energy spectra, in-plane angular correlations, and multiplicities are all reasonably well described by the Monte Carlo CASCADE calculations requiring spin-dependent level densities. The magnitude of the adjustments in the yrast line

position suggests deformation effects at high spin for the ^{56}Ni composite system in agreement with very recent γ-ray spectroscopy data obtained at much lower spins [4]. The extent to which the resonant behavior is responsible to the observed nuclear deformation is still an open question. To resolve this issue, more exclusive data are needed at off-resonance energies. The extracted deformability parameters for ^{28}Si+ ^{28}Si are consistent with the reanalysis of previously published ^{30}Si+ ^{30}Si data. We conclude that mass-symmetric systems do favor the onset of deformation effects at high angular momenta for highly stretched configurations to explain the observed α-particles evaporation spectra. Work is in progress, including out-of-plane correlations measurements, to study the same reactions with the ICARE multidetector array at even higher bombarding energies [25].

ACKNOWLEDGMENTS

This work is based upon the Ph.D. thesis of M. Rousseau, Université Louis Pasteur, Strasbourg, 2000. We would like to thank the staff of the VIVITRON for providing us with good stable beams, J. Devin and C. Fuchs for the excellent support in carrying out these experiments. Particular appreciation to M.A. Saettel for preparing the targets, and to J.P. Stockert and A. Pape for assistance during their RBS measurements is acknowledged. One of us (M.R.) would like to acknowledge the Conseil Régional d'Alsace for the financial support of his Ph.D. thesis work. This work was sponsored by the French CNRS/IN2P3, and by CNRS/NSF and CNRS/CNpq collaboration programs, and also in part by the U.S. DOE under Grant No. DE-FG03-96-ER40981.

[1] S.J. Sanders, A. Szanto de Toledo, and C. Beck, Phys. Rep. **311**, 487 (1999), and references therein.
[2] R.W. Zurmühle, P. Kutt, R.R. Betts, S. Saini, F. Haas, and O. Hansen, Phys. Lett. **129B**, 384 (1983).
[3] R.R. Betts, B.B. Back, and B.G. Glagola, Phys. Rev. Lett. **47**, 23 (1981); R.R. Betts, S.B. DiCenzo, and J.F. Petersen, Phys. Lett. **100B**, 117 (1981).
[4] D. Rudolph *et al.*, Phys. Rev. Lett. **82**, 3763 (1999); Eur. Phys. J. A **4**, 115 (1999).
[5] C.E. Svensson *et al.*, Phys. Rev. Lett. **79**, 1233 (1997); **80**, 2558 (1998); **82**, 3400 (1999).
[6] D. Rudolph *et al.*, Phys. Rev. Lett. **80**, 3018 (1998).
[7] R. Nouicer *et al.*, Phys. Rev. C **60**, 041303(R) (1999).
[8] C. Beck *et al.*, Phys. Rev. C **63**, 014607 (2001).
[9] G. Viesti, B. Fornal, D. Fabris, K. Hagel, J.B. Natowitz, G. Nebbia, G. Prete, and F. Trotti, Phys. Rev. C **38**, 2640 (1988).
[10] I.M. Govil, J.R. Huizenga, W.U. Schröder, and J. Töke, Phys. Lett. B **197**, 515 (1987).
[11] G. La Rana *et al.*, Phys. Rev. C **37**, 1920 (1988); **40**, 2425 (1989).
[12] J.R. Huizenga, A.N. Behkami, I.M. Govil, W.U. Schröder, and J. Töke, Phys. Rev. C **40**, 668 (1989).
[13] D.K. Agnihotri, A. Kumar, K.C. Jain, K.P. Singh, G. Singh, D. Kabiraj, D.K. Avasthi, and I.M. Govil, Phys. Lett. B **307**, 283 (1993).
[14] I.M. Govil *et al.*, Phys. Rev. C **57**, 1269 (1998).
[15] D. Bandyopadhyay, S.K. Basu, C. Bhattacharya, S. Bhattacharya, K. Krishan, A. Chatterjee, S. Kailas, A. Navin, and A. Shrivastava, Phys. Rev. C **59**, 1179 (1999).
[16] I.M. Govil, R. Singh, Ajay Kumar, G. Singh, S.K. Kataria, and S.K. Datta, Phys. Rev. C **62**, 064606 (2000).
[17] I.M. Govil, R. Singh, A. Kumar, S.K. Datta, and S.K. Kataria, Nucl. Phys. **A674**, 377 (2000).
[18] D. Mahboub *et al.*, Phys. Rev. C (to be published); Ph.D. thesis, Strasbourg University, Report No. CRN 96-36, 1996.
[19] N.G. Nicolis and D.G. Sarantites, Phys. Rev. C **40**, 2422 (1989).
[20] C. Bhattacharya, M. Rousseau, C. Beck, V. Rauch, D. Mahboub, R. Nouicer, R.M. Freeman, O. Stezowski, S. Belhabib, A. Hachem, E. Martin, A. Dummer, S.J. Sanders, and A. Szanto de Toledo, Nucl. Phys. **A654**, 841c (1999).
[21] M. Rousseau *et al.*, in *Proceedings of the 7th International Conference on Clustering Aspects of Nuclear Structure and Dynamics*, Rab, Croatia, 1999, edited by Z. Basrak, R. Caplar, and M. Korolija (World Scientific, Singapore, 2000), p. 189.
[22] C. Beck *et al.*, Rice. Sci. Educatione Permanente, Suppl. **115**, 407 (2000).
[23] C. Bhattacharya *et al.*, Pramana, J. Phys. **57**, 203 (2001).
[24] M. Rousseau *et al.*, Ric. Sci. Educatione Permanente, Suppl. **117**, 370 (2001).
[25] M. Rousseau, Ph.D. thesis, Strasbourg University, Report No. IReS 01-02, 2001 (unpublished); G. Bélier, Ph.D. thesis, Strasbourg University, Report No. CRN 94-34, 1994 (unpublished); T. Bellot, Ph.D. thesis, Strasbourg University, Report No. IReS 97-35, 1997 (unpublished).
[26] P. Decowski, E.A. Bakkum, P.F. Box, K.A. Griffioen, R. Kamermans, and R.J. Meijer, Phys. Rev. C **37**, 2495 (1988).
[27] R.J. Meijer *et al.*, Phys. Rev. C **44**, 2625 (1991).
[28] F. Pühlhofer, Nucl. Phys. **A280**, 267 (1977).
[29] S.B. DiCenzo, J.F. Petersen, and R.R. Betts, Phys. Rev. C **23**, 2561 (1981).
[30] Y. Nagashima *et al.*, Phys. Rev. C **33**, 176 (1986).
[31] M.F. Vineyard *et al.*, Phys. Rev. C **41**, 1005 (1990).
[32] H. Dumont *et al.*, Nucl. Phys. **A435**, 301 (1985).
[33] E. Bozek *et al.*, Nucl. Phys. **A451**, 171 (1986).
[34] Arnold J. Sierk, Phys. Rev. C **33**, 2039 (1986).
[35] M.F. Vineyard *et al.*, Phys. Rev. C **49**, 948 (1994).